Mechanical Systems and Signal Processing 98 (2018) 78–90

Contents lists available at ScienceDirect

Mechanical Systems and Signal Processing

journal homepage: www.elsevier.com/locate/ymssp

Impedance measures in analysis and characterization of multistable structures subjected to harmonic excitation

Ryan L. Harne *, Benjamin A. Goodpaster

Department of Mechanical and Aerospace Engineering, The Ohio State University, Columbus, OH 43210, USA

ARTICLE INFO

Article history:
Received 17 October 2016
Received in revised form 24 February 2017
Accepted 25 April 2017

Keywords:
Multiple degrees-of-freedom system dynamics
Multistable
Post-buckled
Nonlinear oscillations
Impedance

ABSTRACT

Structural components susceptible to adverse, post-buckled dynamic behaviors have long challenged the success of applications requiring lightweight, slender curved structures, while researchers have begun to leverage such bistable systems in emerging applications for novel energy attenuation and shape-changing properties. To expedite development and deployment of these built-up platforms containing post-buckled constituents, efficient approaches are required to complement time-consuming full-field models in the prediction of the near- and far-from-equilibrium dynamics. This research meets the need by introducing a semi-analytical model framework to enable the characterization of steady-state responses in multi degree-of-freedom (DOF) and multistable structural systems subjected to harmonic excitation. In so doing, the pathway for assessing impedance measures is created here so as to identify how energy travels and returns within built-up multistable structures. Verified by simulations and qualitatively validated by experiments, the analysis is shown to accurately reproduce both near- and far-from-equilibrium responses including different classes of energetic snap-through dynamics that only exist in such multistable structures. A first look at the impedance measures of different dynamic regimes reveals a connection between damping in multistable structures and the sustainability of far-from-equilibrium oscillations.

1. Introduction

Modern, built-up structural systems are designed closer than ever to the margins of safety using slender structural components with the intent to achieve greater efficiency, functionality, and performance, all at a minimum of cost and weight. Whether the application is for lightweight spacecraft [1], fiber-based automotive components [2], hypersonic aircraft [3], or tensegrity civil structures [4], the use of such flexible structural members promotes the onset of nonlinear dynamic phenomena [5], ranging from small perturbations away from ordinary linear dynamic response patterns [6] to post-buckled "snap-through" events that compromise performance and integrity [7].

The wide-ranging, practical importance of these built-up structural systems, i.e. structures possessing many degrees-of-freedom (DOF), has motivated efforts to identify the prime nonlinearities involved and to predict and characterize the subsequent dynamic responses. To this latter end, high-fidelity models are often developed, typically facilitated by the finite element (FE) method. Yet, the mass, stiffness, and damping constants that populate the FE matrices must be identified which is challenged by the presence of nonlinearities. Therefore, experimental practices for nonlinear parameter identification have

* Corresponding author.
E-mail address: harne.3@osu.edu (R.L. Harne).

http://dx.doi.org/10.1016/j.ymssp.2017.04.036
0888-3270/

been articulated by delli Carri and Ewins [8] and Spottswood and Allemang [9,10] while recently emerging experimental techniques using laser- and high-speed-video-based data are introducing new avenues for extracting such needed information [11,12]. These advancements open the door for FE models to probe the nonlinear dynamic responses, while concurrent efforts have shown that reduced order modeling can considerably enhance the efficiency of such simulations [13,14]. Although these works establish methodologies of great promise, the reliance on time-domain FE simulation nevertheless consumes considerable time and computational resources due to the need to significantly refine time-steps in order to accurately reproduce nonlinear behaviors [15], thus limiting the contribution of such methods on nonlinear structural system development and deployment to specific case studies.

In contrast to time-stepping simulation methods, semi-analytical methods are able to predict the complex dynamic responses of nonlinear structures using orders-of-magnitude less computational expense, albeit with a fidelity not as true as full-field numerical simulation. On the other hand, the "cost" of these analytical methods is largely proscribed by the difficulty in formulating approximate theories and solution methods that facilitate dynamic response predictions at an accuracy useful for engineering system design. The assumptions of steady-state or stochastic response, single DOF system, or single physics are often applied to enable the semi-analytical study of nonlinear structures with experimentally-relevant fidelity [16] since formulating a theoretical tool that sufficiently addresses a combination of nonlinear features, multiple physics, and multi DOF is challenging. Yet, researchers have recently shown that such analytical models may predict important and unique nonlinear phenomena such as post-buckling bifurcation behaviors [17], intriguing detached resonance curves [18], transient and persistent snap-through buckling [19–21], and internal resonance [22]. These are also examples of far-from-equilibrium nonlinear responses, which are in general much more difficult to predict than weakly nonlinear dynamics that are small perturbations from underlying linear behavior [23]. This is because the guiding assumptions in the theoretical developments must be established upon firm bases due to large deviations from linearity lest the predictions be devoid of utility. Such bases are typically provided by empirical evidence or intuitive reasoning [24].

Steps to advance semi-analytical methods to predict the dynamic response of more complex nonlinear structures operating under less ideal conditions are being pursued. In particular, researchers have recently formulated analytical methods to predict the excited, nonlinear response of multi DOF structures modeled as coupled mass-spring-damper sub-systems [25–28]. The extension to studies of multi DOF systems is of prime, practical importance. Such perspective introduces opportunity to investigate how power flows through excited, nonlinear structural systems built-up from many constituents [29]. Exploring energetic measures is relevant since a sub-system vulnerable to high deformations given a certain energy input must be identified at an early stage of development lest it result is large, far-from-equilibrium behaviors when deployed. Yet, these recent advancements [25–28] are limited to considering certain weak nonlinearities in the model formulation that permit small deviations away from linearity and thus cannot uncover behaviors that cause far-from-equilibrium responses such as snap-through.

Indeed, the number of examples where slender beams, panels, or multi-body systems possessing one or more bistable, buckled, or slightly curved constituents are used in applications is large and growing. The contexts range from mechanical metamaterials [30], shape-morphing structures [31], bifurcation-based sensors [32,33], to thermally-stressed aircraft panels [3], including the example shown in Fig. 1(a). As such, the important snap-through dynamic of these multistable structures may become activated.

To appreciate this critical dynamic response, displacement measurements of the three DOF experimental system studied in this report are shown in Fig. 1(b) where a slowly changing frequency of harmonic force excitation into beam 1 induces a sudden onset of snap-through dynamics near time 620 s at which point the instantaneous excitation frequency is around 17 Hz, in other words slightly less than the lowest natural frequency of the system around 18 Hz. Activation of snap-through in beam 1 causes a cascade of the behavior into the system, ultimately resulting in all three beams snapping through. One may perceive an analogy of this experimental evidence to the cascading of strong nonlinear dynamic response through a realistic post-buckled panel system such as that shown in Fig. 1(a) on the aircraft skin. The proportionality between stress and strain indicates that the onset of aperiodic or persistent snap-through buckling is a clear detriment to long-term system integrity [3], in addition to the adverse impacts on other performance traits including aerodynamics and reusability.

Consequently, a particular need in state-of-the-art development of semi-analytical methods for computationally-efficient prediction of the excited dynamics of nonlinear structures is the accommodation of *multi DOF systems including post-buckled constituents*. Because such dynamics potentially include *far-from-equilibrium* behaviors, the prior theoretical formulations are not applicable due to foundations of development which presume the existence of weak nonlinearities relatively near to dynamic equilibria [25–28].

Therefore, the aim of this research is to provide a new foundation for the analytical study of excited multi DOF structures including constituents which may be post-buckled, and thus possibly driven to undergo snap-through oscillations. In so doing, this study also introduces a means to uncover energetic measures of importance in the design and development of harmonically-excited nonlinear structures via a first evaluation of the *impedance* of post-buckled constituents assembled into a system. By this approach and using a fundamental understanding of traditional linear impedance-based analysis, this report gives the first articulation of multi DOF, post-buckled system impedances that serve as signs for the existence of near- and far-from-equilibrium dynamics.

This paper presents these new outlooks and results via the following organization. The next section describes the archetypal dynamic system under consideration as it relates to the experimental platform developed for laboratory assessment and

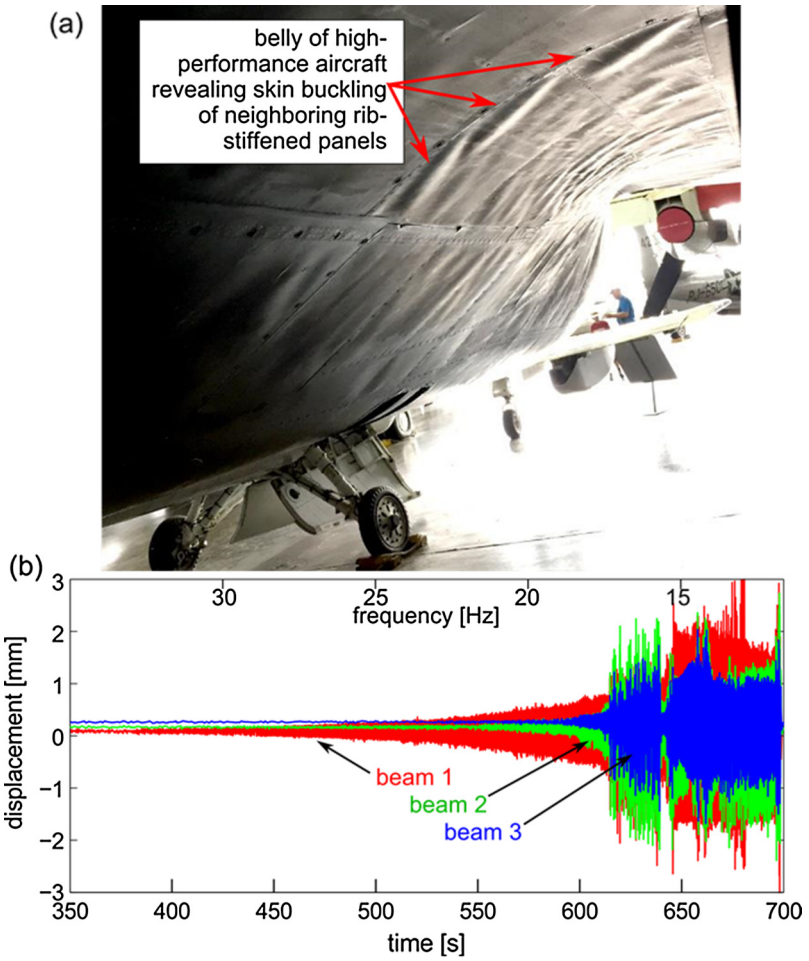

Fig. 1. (a) Photograph taken by the authors of a Lockheed YF-12A at the National Museum of the U.S. Air Force at Wright-Patterson AFB, Ohio, USA, revealing skin buckling on neighboring rib stiffened panels. (b) Measurements of the experimental system of this research showing an onset of snap-through buckling dynamics as a slow change in the single frequency of force excitation that drives beam 1 approaches 17 Hz which is slightly less than the lowest natural frequency of the system around 18 Hz and exemplifies the softening nonlinear of the multistable structure.

to practical embodiments of multi DOF structural systems containing post-buckled constituents. Then, the model formulation and its semi-analytical solution approach are described. Discussions are then provided that compare analytical predictions, numerical simulations, and experimental measurements to validate the model and to characterize first observations of the influences of impedance measures on the onset of nonlinear dynamic phenomena in built-up, post-buckled structural systems.

2. Multi DOF system description

2.1. Lumped-parameter system definition

A harmonically-excited, nonlinear, n DOF system is considered where each generalized coordinate is coupled to all other DOF. Without loss of generality, a three DOF system is specifically examined here, shown schematically in Fig. 2(a), in accordance with the experimental platform discussed in Section 2.2 and by virtue of the research motivation shown in Fig. 1(a). Fig. 2(b) provides a schematic of the i^{th} DOF in the system and the forces acting on the mass element. The m_i, c_i, and $k_{i,h}$ are, respectively, the mass, viscous damping constant, and linear spring stiffness for the i^{th} generalized coordinate. The corresponding generalized force is $f_i(t)$. Linear elastic coupling exists between all pairs of coordinates. For instance, a spring force between the i^{th} and $(i+4)^{th}$ coordinates is due to the relative deformation $x_{i+4}-x_i$ of spring with stiffness $k_{i+4,i}$. Local nonlinearity exists between each generalized coordinate and a respective ground reference according to a nonlinear force given by $-k_{i,i}p_ix_i+k_{NL,i,i}x_i^3$ for the i^{th} generalized coordinate. The force $k_{NL,i,i}x_i^3$ is representative of large deformation such as

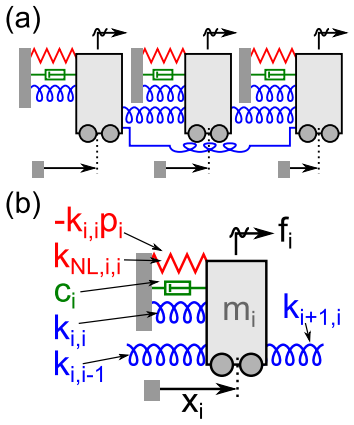

Fig. 2. (a) Lumped-parameter schematic of three DOF system examined in this research. (b) Coupling elements and forces acting on each DOF of the system.

stretching in a beam, while the force $-k_{i,i}p_ix_i$ is associated with loads that reduce the linear stiffness to such extent that it may become negative. Both of these influences are commonly encountered in the study of axially compressed (possibly post-buckled) structural members undergoing transverse vibration [5], which is the focus of this study and motivation for model definition. While the nonlinearities investigated in this report are local and pertain only to elastic effects according to the specific research motivations, the analytical procedure established can readily be employed to account for other local and global elastic and dissipative nonlinearities, since the present theoretical foundation builds upon a method articulated by Spanos [34] that is amenable to such broader classes of nonlinearities.

2.2. Experimental setup description

The three DOF experimental platform examined in this research is composed in a way to amply realize the lumped parameter assumptions exemplified in the schematic of Fig. 2(a), while it effects a less complex architecture than a genuine panel system composed with post-buckled constituents, Fig. 1(a). A photograph of the platform is shown in Fig. 3(a). Three simply-supported, spring steel beams are mounted to an optical isolation table (Newport Smart Table UT2). One end of each beam is able to be axially compressed to different extents via a fine-threaded load screw that moves the simple support end. The axial compression permits the negative linear force realized in the model by the terms $-k_{i,i}p_ix_i$ since it reduces the linear stiffness in proportion to the nearness to the fundamental, critical Euler load [5]. Large deflection of the beams (with respect to the beams' thicknesses, all approximately 0.635 mm) permits the cubic nonlinear restoring force $k_{NL,i,i}x_i^3$ [35]. In this study, each beam is compressed to an extent to induce a weak post-buckling so that $p_i > 1$. For instance, the largest peak-to-peak distance between post-buckled stable equilibria considered here (without beam-to-beam coupling springs) is 3 mm which contrasts with the beam's length of 257 mm and thickness 0.635 mm. Thus, the beams are buckled only in the fundamental mode shape.

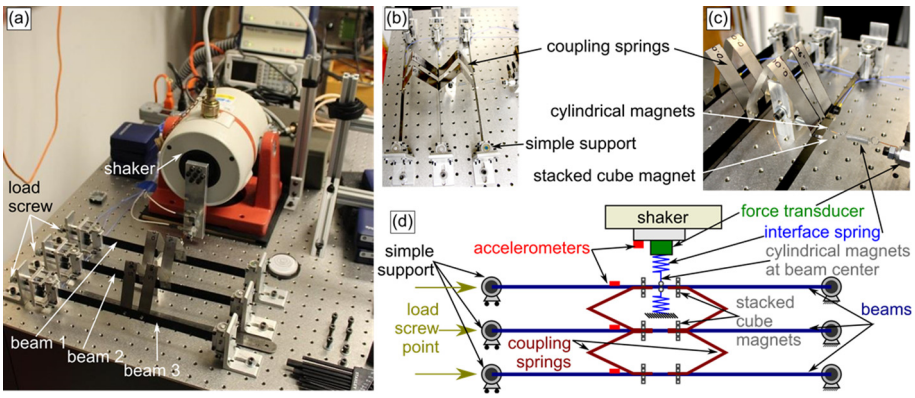

Fig. 3. (a) Photograph of experimental prototype of three beam system coupled via bent springs. The beam 1 is driven by the shaker via the relative deformation of the interfacing springs and a rigid bar extending from the shaker. (b) Close-up photograph of the coupling springs and simple supports. (c) Close-up photograph of the attachment between the shaker and beam 1. (d) Top-down view schematic of the experimental setup.

By virtue of the roller ball bearing design (McMaster 8600N3), the simple supports effect viscous damping forces for moderate to high amplitudes of beam oscillation but exert friction-like force characteristics for very small beam oscillations [36]; the latter condition is not within the scope of this research, where the focus is instead on conditions that promote meaningful amplitudes of dynamic response. Nearest neighboring beams are elastically coupled at locations close to their center points by bent spring steel springs, Fig. 3(b), that provide a linear restoring force for the small deformations. This coupling is chain-like in nature but lacks the global coupling characteristic of Fig. 2(a); in other words, the global coupling spring of stiffness $k_{1,3} = k_{3,1}$ in the more general model schematic is not present in the experimental platform. The coupling springs are secured between beams by high-strength, miniature cube magnets that are slightly visible in Fig. 3(c). Between each beam pair, the coupling spring pair is slightly offset from the beam centers to best promote dynamic behaviors associated only with the lowest order mode for pre- and post-buckled conditions [37]. The "beam 1" nearest to the shaker is excited via a pair of tension interfacing springs that provide connection to the electrodynamic shaker (LDS V408). The interfacing springs attach to beam 1 using high-strength, miniature cylindrical magnets soldered to the spring ends. Due to the height difference between the beam centers and shaker axis, a thick and rigid aluminum bar is used to convert the motions of the shaker into parallel motions at the level of the beam centers, so that forces acting on beam 1 via deformation of the interfacing spring are aligned with the transverse motion of the beam center.

To excite the system, a vibration controller (Vibration Research VR9500) provides a feedback-controlled signal to a power amplifier (Crown XLS1500) that drives the shaker. The shaker acceleration characteristics are governed via the controller and reference accelerometer (PCB 333B40) mounted on the shaker attachment bar. A force transducer (PCB 208C01) is attached between the shaker bar and interfacing springs to measure the real-time force delivered to beam 1. Although the controller maintains acceleration according to the reference accelerometer, it was found that under steady-state operations the input force was dominated by the instantaneous harmonic excitation frequency with nonlinear harmonic force generation never exceeding about 20% of the force amplitude associated with the fundamental frequency, thus ensuring strong agreement with the single-frequency force excitation description used in the analysis. Experimentally, a miniature accelerometer (PCB 352A24) is attached on each beam at approximately 42% of the length from a simple supported end. Data acquisition hardware (National Instruments) accepts the signals from these five sensors which are then post-processed (MATLAB) for time- and frequency-domain assessment purposes.

By being weakly buckled in the fundamental mode and with the present focus of excitation frequencies only around the lowest three linear natural frequencies, the dynamic responses of the three beam system occur strictly in spatial distributions proportional to the fundamental modes. Thus, higher-order mode buckling is not observed in the data collected and evaluated in this investigation. Consequently, as a first approximation, such careful system composition and observed experimental behaviors enable the reduction of a three coupled-beam, distributed parameter system model into an equivalent lumped parameter system model on the basis of Galerkin's method and Newton's 2nd law [5,35]. The equivalent lumped parameter system is schematically shown in Fig. 2(a), noting that in the experimental platform the global coupling spring stiffness $k_{1,3} = k_{3,1} = 0$ and the excitation forces $f_2 = f_3 = 0$.

3. Analytical model formulation

Considering the schematics shown in Fig. 2, generalized to the n DOF system, the use of Newton's second law of motion leads to a system of governing equations described by

$$[M]\underline{\ddot{x}} + [C]\underline{\dot{x}} + [K]\underline{x} + \underline{N}(\underline{x}) = \underline{F} \tag{1}$$

The underline denotes a vector while the [ ] brackets denote a matrix. In (1), the terms are

$$[M] = diag[m_i], [C] = diag[c_i], [K]_{ih} = \begin{cases} \sum_{h=1}^{n} k_{i,h}; i = h \\ -k_{i,h}; i \neq h \end{cases} \tag{2}$$

$$\underline{x} = [x_1, x_2, \cdots, x_n]^T, \underline{F} = [f_1, f_2, \cdots, f_n]^T \tag{3}$$

where T is the transpose operator. The nonlinear forces $\underline{N}(\underline{x})$ considered in this study are

$$\underline{N}_i = -k_{i,i}p_i x_i + k_{NL,i,i}x_i^3 \tag{4}$$

while, as indicated in Section 2.1, the analytical method described below can readily be extended to enable exploration of local and global elastic and dissipative nonlinearities.

3.1. Linear response

To examine the linear system dynamic response, one must determine the equilibria $\underline{x}^*$ given that post-buckled configurations may not satisfy the trivial case of $\underline{x}^* = \underline{0}$ that is common to weakly nonlinear n DOF systems. The equilibria are therefore determined by solving

$$[K]\underline{x}^* + \underline{N}(\underline{x}^*) = \underline{0} \tag{5}$$

Due to the nonlinearity of $\underline{N}(\underline{x}^*)$, there may be multiple equilibria identified from (5) if one or more constituents in the system is post-buckled. Then, the transformed coordinate is defined $\underline{y} = \underline{x} - \underline{x}^*$ and substituted into (1) to yield

$$[M]\ddot{\underline{y}} + [C]\dot{\underline{y}} + [K]\underline{y} + [K]\underline{x}^* + \underline{N}(\underline{y} + \underline{x}^*) = \underline{F} \tag{6}$$

where the components of the nonlinear terms are

$$\underline{N}(\underline{y} + \underline{x}^*)_i = -k_{i,i}p_i y_i - k_{i,i}p_i x_i^* + k_{NL,i,i}y_i^3 + k_{NL,i,i}(x_i^*)^3 + 3k_{NL,i,i}(x_i^*)^2 y_i + 3k_{NL,i,i}x_i^* y_i^2 \tag{7}$$

The elements of (7) are concisely expressed using

$$\underline{N}(\underline{y} + \underline{x}^*)_i = [K_L]_{i,i}y_i + \underline{N}(\underline{x}^*)_i + (\underline{K}_{NL})_i \tag{8}$$

where

$$[K_L] = diag[-k_{i,i}p_i + 3k_{NL,i,i}(x_i^*)^2] \tag{9}$$

$$\underline{N}(\underline{x}^*)_i = -k_{i,i}p_i x_i^* + k_{NL,i,i}(x_i^*)^3 \tag{10}$$

$$(\underline{K}_{NL})_i = 3k_{NL,i,i}x_i^* y_i^2 + k_{NL,i,i}y_i^3 \tag{11}$$

Using (5) and considering the expansion of (8) and definitions (9)(11), (6) is rewritten to be

$$[M]\ddot{\underline{y}} + [C]\dot{\underline{y}} + \{[K] + [K_L]\}\underline{y} + \underline{K}_{NL} = \underline{F} \tag{12}$$

The governing equations (12) are therefore defined around an equilibrium for $\underline{y} = \underline{0}$. As such, the linearized form of (12) is

$$[M]\ddot{\underline{y}} + [C]\dot{\underline{y}} + \{[K] + [K_L]\}\underline{y} = \underline{F} \tag{13}$$

whose undamped linear eigenvalue problem of the homogeneous form of (13) is solved under the assumption of harmonic response $\underline{y} = \underline{Y}e^{\lambda t}$. Likewise, the linear forced response of (13) is computed assuming harmonic excitation

$$\underline{F} = \underline{f}e^{j\omega t} \tag{14}$$

where $j = \sqrt{-1}$, that induces a harmonic response

$$\underline{y} = \underline{Y}e^{j\omega t} \tag{15}$$

The use of (14) and (15) towards predicting the forced response is conducted with the understanding that the actual, measurable responses of the system are the real components of (14) and (15).

For weakly nonlinear system dynamics, the nonlinear forced response of a multi DOF structure may not be considerably different than the solution to (13). Yet, for systems that contain one or more post-buckled constituents, the responses are inherently "far" from the linear equilibrium $\underline{x}^* = \underline{0}$. Therefore, a new approach is required to predict and explore the forced responses of such strongly nonlinear systems.

3.2. Nonlinear forced response

To this end, one returns to (1) and invokes procedures of stochastic or harmonic linearization [34,38]. An equivalent system to (1) is introduced using

$$[M]\ddot{\underline{x}} + [C]\dot{\underline{x}} + \{[K] + [K_e]\}\underline{x} = \underline{F} \tag{16}$$

For generalized coordinates that are coupled in a chain-like configuration via relative displacements

$$\underline{N}(\underline{x})_i = \sum_{h=1}^{n} g_{i,h}(w_{i,h}), w_{ih} = \begin{cases} x_i - x_h, i \neq h \\ x_i, i = h \end{cases} \tag{17}$$

and g_{ih} is an odd function of w_{ih}. Then the component $[K_e]_{i,h}$ is computed from

$$[K_e]_{i,h} = \frac{\langle g_{i,h}w_{i,h}\rangle}{\langle w_{i,h}^2\rangle} \tag{18}$$

where the brackets denote the mathematical expectation. Example coupling phenomena that do not satisfy the property of being chain-like include couplings proportional to the products of coordinate motion rather than due to relative motion differences [34]. This is not a considerable limitation to the approach currently developed since a significant number of practical problems in structural dynamics involve such chain-like couplings among generalized coordinates [28,39].

In general, the components of $[K_e]_{i,h}$ are functions of unknown constants associated with the assumed solution for each generalized coordinate contributing to the computation of (18) for the relative motion w_{ih}. For the local nonlinearity encountered in Fig. 1(b), the $[K_e]$ is diagonal and $w_{i,i} = x_i$.

A specific case is useful to engage the method in greater detail. Consider a harmonic excitation (14). Using the coordinates $\underline{x}$ and respecting the general case that the equilibria may not be $\underline{x}^* = \underline{0}$, an appropriate assumed solution must account for non-zero generalized coordinate bias as well as oscillations according to the anticipated steady-state response (15). Consequently, one assumes

$$\underline{x} = \underline{q} + \underline{r}e^{j\omega t} \tag{19}$$

where in general the biases $\underline{q}$ are real while the amplitudes $\underline{r}$ are complex. This approach was conceived in Ref. [34] to investigate the dynamics of structures with asymmetric nonlinearities undergoing dynamics near to equilibrium, but has not yet been considered as a strategy for analyzing post-buckled n DOF systems that may include both near-to- and far-from-equilibrium dynamics. Using (19), the components (18) are averaged over a period of the harmonic excitation, $T = 2\pi/\omega$. Substituting (19) into (18) and averaging over T, one obtains

$$[K_e]_{i,h} = \begin{cases} -k_{i,i}p_i + k_{NL,i,i}\left[3q_i^2 + \frac{3}{4}r_i^2\right], i = h \\ 0, i \neq h \end{cases} \tag{20}$$

In (20), the approximation is made that $\frac{9}{2}q_i^2 - \frac{7q_i^4}{2q_i^2 + r_i^2} \approx 3q_i^2$ which agrees well to numerical simulation results and previous related derivation [20] according to the present focus on symmetric post-buckled sub-systems. Upon substitution of (19) into (16), one obtains

$$\{-\omega^2[M] + j\omega[C] + [K]\}\underline{r}e^{j\omega t} + \left[K_e(\underline{q},\underline{r})\right]\underline{r}e^{j\omega t} + \left\{[K] + \left[K_e(\underline{q},\underline{r})\right]\right\}\underline{q} = \underline{F}e^{j\omega t} \tag{21}$$

The time-harmonic terms $e^{j\omega t}$ in (21) are independent of the time-independent terms that are products with the biases $\underline{q}$. As such, to uniquely satisfy (21), one must simultaneously solve (22) and (23).

$$\left\{[K] + \left[K_e(\underline{q},\underline{r})\right]\right\}\underline{q} = \underline{0} \tag{22}$$

$$\{-\omega^2[M] + j\omega[C] + [K]\}\underline{r} + [K_e(\underline{q},\underline{r})]\underline{r} = \underline{F} \tag{23}$$

To address (23), one introduces $[\Lambda] = -\omega^2[M] + j\omega[C] + [K]$. Then, Eq. (23) is expressed using [27]

$$[\Lambda]\underline{r} = \underline{F} - [K_e]\underline{r} \tag{24}$$

where the $(\underline{q},\underline{r})$ dependence of $[K_e]$ is dropped for brevity. Solution to the components r_i in (24) is obtained by Cramer's Rule [40].

$$r_i = \frac{\det\begin{bmatrix} \Lambda_{1,1} & \cdots & & \Lambda_{1,n} \\ \Lambda_{2,1} & \cdots & & \Lambda_{2,n} \\ \vdots & \vdots & \underline{F} - [K_e]\underline{r} & \vdots \\ \Lambda_{n,1} & \cdots & & \Lambda_{n,n} \end{bmatrix}}{\det[\Lambda]} \tag{25}$$

The notation in (25) is that the i^{th} column of the numerator is replaced with $\underline{F} - [K_e]\underline{r}$.

For the k DOF that include a nonlinear local coupling to the ground reference, the Eqs. (22) and (25) provide a coupled set of $2k$ algebraic equations ($k \leqslant n$) to solve. The generalized coordinate amplitudes and biases for the remaining DOF that involve only linear local and global couplings may be solved for in sequence, using the appropriate portions of (25), once the respective amplitudes and biases for the nonlinear coordinates are found from (25).

Having obtained the complex response amplitudes $\underline{r}$, the impedances are computed using

$$Z_{i,h} = \frac{F_h}{j\omega r_i} \tag{26}$$

where $i = h$ are complex input (or drive-point) impedances and $i \neq h$ are complex transfer impedances. The real (imaginary) parts of the impedances denote the inhibition of energy transfer (effectiveness of energy reciprocation) [41].

3.3. Solution method for semi-analytical results

Eqs. (22) and (25) represent $2k$ nonlinear equations that are solved to assess the influences of parameters and harmonic excitation features upon the dynamics induced in the nonlinear n DOF system. In this research, a trust-region-dogleg algorithm (nonlinear least squares cost function minimization) via the *fsolve* command in MATLAB software is used to numer-

ically solve the equations. This approach is capable of solving equations with complex variables, like (25). On the other hand, convergence is observed to be slow. Hence in this research the real and imaginary parts of (25) are solved as separate equations. While this may appear to delay the process of analytical prediction since the number of equations increases from $2k$ to $3k$, in fact it is found to significantly expedite the solution procedure. At each increment of independent variable the equations are solved 20 times, where 25% of initial guesses are randomly selected values among the orders of magnitude of values represented by the dynamics, 25% of initial guesses are randomly perturbed values from the underlying linear response for the same independent variable, and 50% of initial guesses are randomly perturbed values from the solution result from the prior independent variable. This method of seeding initial guesses is found to be robust to locating the steady-state dynamic regimes and is about six or more times faster than direct numerical integration of the governing equations (also undertaken for analytical model verification purposes).

4. Results and discussions

4.1. Model verification and experimental comparison

System identification of the experimental system is carried out to approximate the equivalent lumped parameter values that constitute the three DOF system model. Here, the beams are termed beam 1, 2, and 3, as labeled in Fig. 3(a). Before the beams are coupled, free vibration responses are recorded to approximate damping constants c_i and linear natural frequencies ω_i. The fundamental mode contributions of linear, local stiffness $k_{i,i}$ for the beams are computed from basic theory [42]. Each mass, including contributions due to fundamental mode motions [42], attached magnets, and accelerometers, is approximately m_i=15 g. These estimates enable the determination of axial compressive load parameters p_i via $2k_{i,i}(p-1)=m_i\omega_i^2$, since $p_i>1$ for all beams considered in this study [5]. Note that this parametric selection $p_i>1$ is motivated by a greater experimental vision, such as the panel structure in Fig. 1(a), and is not a limitation to the suitability of the analysis developed here. Based on the measurements, the linear, local stiffness of the beams is each about $k_{i,i}$ = 200 N/m while for beam 1 the stiffness is about $k_{1,1}$ = 350 N/m due to the attached tension springs for shaker excitation.

Using the amplitude of the symmetric, statically-stable equilibria $x_i^{\#}$ for each uncoupled beam from the configuration without axial load x_i = 0, the nonlinear stiffnesses $k_{NL,i,i}$ are then computed by $k_{NL,i,i}=k_{i,i}(p_i-1)/(x_i^{\#})^2$. Prior to their attachment to the beams, the stiffnesses of the coupling springs are approximated to be $k_{1,2}=k_{2,1}$ = 35 N/m and $k_{2,3}=k_{3,2}$ = 53 N/m using static load measurements. The generalized forces for beams 2 and 3 are zero. Because the force driving beam 1 is governed by a controlled shaker acceleration and deformation of the tension spring pair, the force is modeled as having a frequency dependent amplitude $|f_1|=k_cA/\omega^2$ where k_c = 150 N/m is the net tension spring stiffness and A is the amplitude of the shaker acceleration. The remaining identified system parameters are given in Table 1, while the forces f_2 and f_3 are zero in accordance with the experiment. Despite extensive system identification efforts, the imperfections from beam to beam, the bearings in the simple supports, and the appreciable number of connections among system members with spring attachments collectively prevent a quantitative comparison of analytical model results to the measurements. Nevertheless as shown below, a good qualitative agreement in trends is plainly observed between analytical an experimental findings. Hereafter, for consistency, the analytical and numerical results are discussed referring to the three DOF as "beams" although only the experimental system properly considers beams.

Fig. 4(a) presents the velocity amplitude for the three beams of the structure when the shaker acceleration amplitude is A = 1.8 m/s^2. The dashed curves are the linear response predictions, the open data points are analytical predictions, and the dots are results from numerical simulations. In an identical way as for experimental data, the simulation results are determined by selecting the spectral component of the fast Fourier transform of the numerically integrated response time series that is equal to the harmonic excitation frequency. According to the symmetric post-buckled configurations of each subsystem and considering the coupling spring stiffnesses with respect to local spring stiffnesses, only one underlying linear response is uncovered for this multi DOF structure. Thus, while there are four states of statically stable equilibria (in fact, two pairs of symmetric configurations), they do not result in significantly different linear forced response. Considering the nonlinear forced response (data points and dots), the resonances are observed to "soften" to lower frequencies than the frequencies of peak response for the linear behavior. Indeed, this is expected because post-buckled structures exhibit softening spectral trends in the low amplitude, nonlinear dynamic regime [5,35], termed "intrawell". The analytical and numerical results are in good agreement as to the quantitative and qualitative deviation of the forced, nonlinear dynamics of the three DOF structure from the respective linear behaviors.

Table 1
Approximate experimental platform system parameters.

beam	c_i [mN.s/m]	$k_{NL,i,i}$ [MN/m^3]	p_i [dim]
1	317	800	1.77
2	198	520	1.65
3	256	1360	1.43

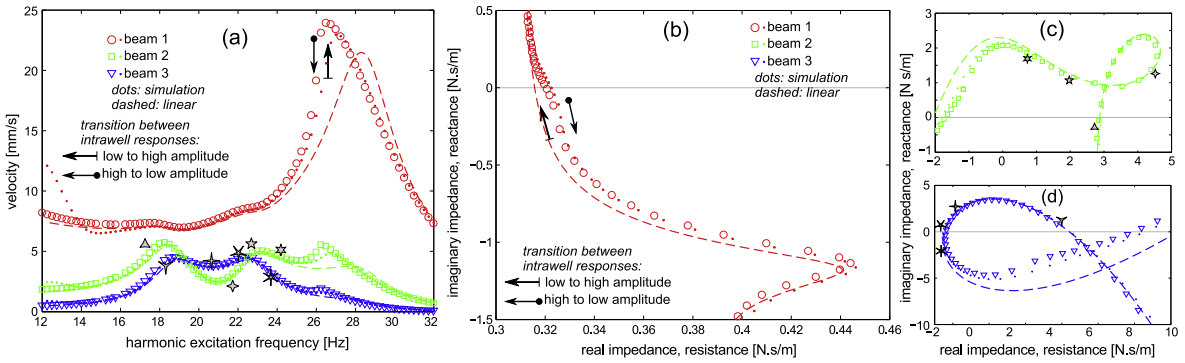

Fig. 4. Analytical, numerical results. (a) Velocity amplitude of the beams as a function of harmonic excitation frequency. (b–d) Trends in impedance around critical frequency regimes for each DOF as denoted by the corresponding curves and symbols provided in (a). Shaker acceleration amplitude $A = 1.8$ m/s^2. Dashed curves are linear response predictions, open data points are analytical predictions, and dots are numerical simulation results.

Fig. 5(a) presents the corresponding measurements of beam velocity amplitude when the shaker acceleration amplitude is $A = 0.95$ m/s^2. Experiments are conducted with the harmonic excitation frequency changing at a rate of 0.03 Hz/s in increasing and decreasing values over the bandwidth shown in the figure. The overall dynamics of the system clearly agrees with the qualitative trends observed in the nonlinear forced responses in Fig. 4(a) as generated by the model. The level of excitation that drives the experimental platform induces a bifurcation at frequency 26 Hz, seen by a sudden jump up (down) in velocity amplitude, for increasing (decreasing) frequency in the slow sweep, for beams 1 and 2. At frequencies away from the important region around the resonances, i.e. outside of about 18 to 32 Hz, the damping in the simple support bearings greatly suppresses system oscillations, which explains the negligible response levels measured in beams 2 and 3 when driven at frequencies outside of this bandwidth. Nevertheless, within the important frequency band, the qualitative agreement between the modeled results and measured data is good. This adds a degree of experimental validation to the numerical verification for the semi-analytical model formulation and solution approach developed in this research.

4.2. Steady-state impedance measures for forced, multistable structures in low amplitude dynamic regimes

In parts (b), (c), and (d), Figs. 4 and 5 present the real and imaginary parts of impedances for beams 1, 2, and 3, respectively. The analytical and numerical results, Fig. 4, are in good agreement as to the ways by which the nonlinear impedance measures differ from those of the underlying linear system (dashed curves). One crossing of zero reactance (imaginary part of impedance), Fig. 4(b), occurs as the driven beam 1 undergoes the resonance around 26 Hz, while two and three zero-crossings in reactance respectively occur for beams 2 and 3 corresponding to resonances/modes, respectively at 18 and 23 Hz, and near to the occurrence of the resonance at 26 Hz. These characteristics are likewise observed in the experimental data, Fig. 5(b–d), where the more dramatic bifurcation at 26 Hz for beam 1 corresponds to a sudden leap of reactance from negative to positive values Fig. 5(b), and vice versa depending on the frequency sweep direction. When reactance vanishes, the management of the input energy in the three DOF system is fully governed by the means for the system to dissipate energy, according to a conservation of energy. Thus, the resistance, real part of impedance, controls the ultimate response amplitudes in such conditions [41]. It is seen that for the low amplitude nonlinear, forced dynamic regime of this multistable structure, Figs. 4 and 5(b–d) reveal that the resistance values are considerable at these resonant states where the reactance

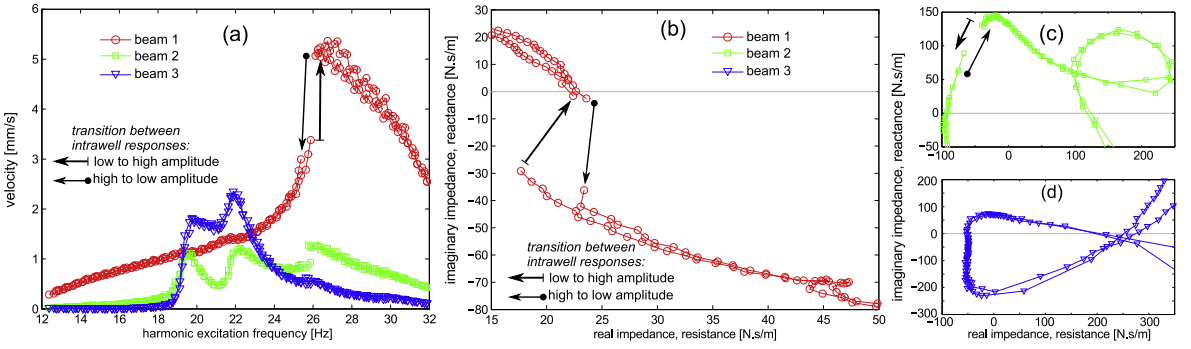

Fig. 5. Experimental results. (a) Velocity amplitude of the beams as a function of harmonic excitation frequency. (b–d) Trends in impedance around critical frequency regimes for each DOF. Shaker acceleration amplitude $A = 0.95$ m/s^2.

vanishes. Thus, when oscillating in the low amplitude dynamic regime, the multi DOF and multistable structure is sufficiently able to manage the input energy via damping mechanisms. As described in the following sub-section of this report, a dramatic change occurs in impedance measures when snap-through dynamics are triggered.

4.3. Characterization of snap-through response in multi DOF structures

Although transfer functions of force to response (or corresponding inverse relationships) have been investigated for weakly nonlinear, multi DOF systems [26–28,39], such qualities have not been uncovered for multistable structures that may oscillate far-from-equilibrium, such as that exemplified in the time series of Fig. 1(b) where snap-through is excited in the experimental platform of this research. Thus, this section firstly verifies and validates the model efficacy in predicting the steady-state dynamics of the multistable structure when harmonically forced and then takes a new look at the ways in which input and transfer impedances are tailored in consequence to the occurrence of snap-through response.

As the amplitude of harmonic excitation driving a post-buckled structure increases, energetic oscillations between the stable equilibria, snap-through, may be triggered [5,14,35]. Consequently, to explore the regime corresponding to the far-from-equilibrium dynamics, the analytical and numerical results, shown in Fig. 6(a), are determined according to a shaker amplitude excitation level $A = 3.8$ m/s^2. In the analytical predictions (open data points), the softening resonance features at high frequencies in the bandwidth plotted are seen to merge into a collective softening behavior that loses distinction from the lower frequency linear resonances around 18 and 23 Hz. The simulations (dots) do not predict such severe distortion in the bandwidth of 20–22 Hz, where instead a softening resonance regime occurs in the numerical results. One explanation for this deviation between analytically and numerically predicted dynamics in the low amplitude nonlinear regime from about 20 to 22 Hz is that the approach to obtain solutions for the analytical model formulation (nonlinear least squares cost function minimization) appears to suggest that the local cost function minima provided by these intrawell behaviors are greater than the minima associated with the higher amplitude nonlinear regime occurring in the same frequency bandwidth; in consequence, the minimization procedure is challenged to identify the low amplitude responses. The authors are pursuing more robust numerical methods and tuning [43] by which such deviations may be overcome in the ongoing development of the analytical model formulation and solution approach.

At low frequencies, the analytical and numerical methods both predict the possible activation of one of two snap-through dynamic regimes, shown according to the considerably greater amplitudes of beam velocity in the frequency band 12–18 Hz and labeled A$*$ and B$*$. Around 14 Hz, each sub-system snaps-through in-phase with the excitation force (to be verified below) while a second possibility occurs around 17 Hz where beam 1 snap-through while beams 2 and 3 undergo a lower amplitude motion at the frequency of the excitation. The analytical and numerical modeling methods are in qualitative agreement as to these trends although the quantitative amplitudes of the respective responses do not exactly agree. As shown below via the experimental time series, this is due to the activation of other-order harmonic oscillations that tailor the response amplitudes proportional to the driving frequency, which is likewise evident in the numerical time series whose spectral response is concisely shown via the data points in Fig. 6(a).

Interestingly, when beam 1 of the experimental platform is driven by shaker acceleration amplitude $A = 9.3$ m/s^2 so as to cause far-from-equilibrium responses at frequencies less than around 18 Hz, the mostly single-periodic dynamics observed

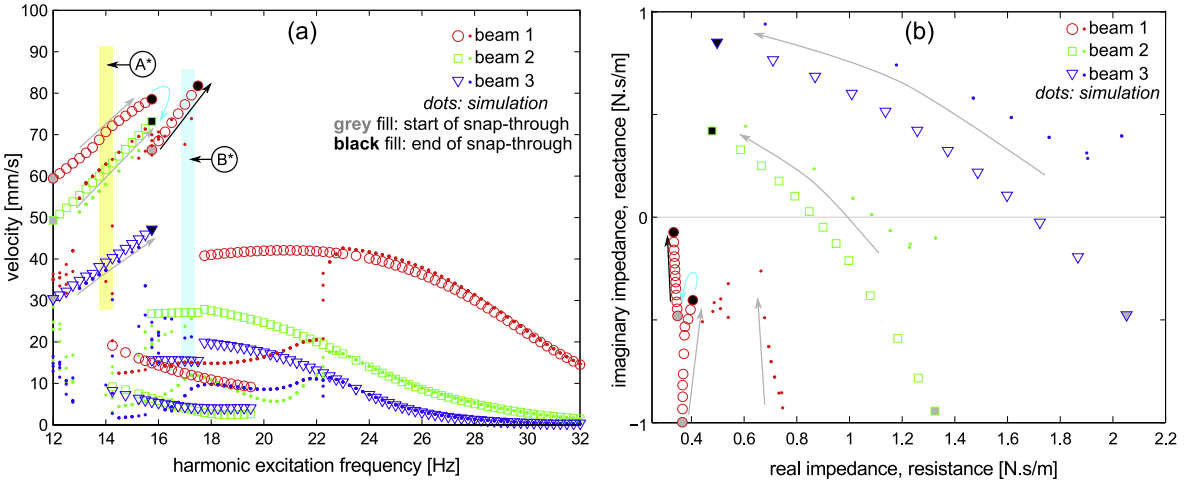

Fig. 6. Analytical, numerical results. (a) Velocity amplitude of the beams as a function of harmonic excitation frequency. (b) Trends in impedance. Only those impedance measures corresponding to snap-through dynamic regimes are shown. Shaker acceleration amplitude $A = 3.8$ m/s^2. Dashed curves are linear response predictions, open data points are analytical predictions, and dots are numerical simulation results. Grey- and black-filled data points respectively correspond to lower and upper bound frequencies of snap-through regimes.

experimentally in Fig. 7(a) are in greater qualitative agreement with the analysis than with numerical simulations. This is because the simulations suggest that a notable proportion of the dynamic behaviors are aperiodic or multi-harmonic, as seen in the more scattered numerical data points in Fig. 6(a) in the lower frequency regime. Comparing the experimental observations from the low amplitude nonlinear dynamic regime to the responses observed when the beam 1 is driven at a the greater level reveals a progression from purely softening nonlinear response trends in Fig. 5(a) to a combination of severe softening nonlinear oscillations at higher frequencies and snap-through dynamics at frequencies below about 18 Hz, as seen in Fig. 7(a). Experimental studies employing excitation at intermediate amplitudes, not shown for sake of brevity, confirm that an evolution exists from one dynamic regime to the next, where the softening low amplitude nonlinear resonances gradually "lean" more and more towards lower frequencies for increasing excitation amplitude, while snap-through is ultimately triggered for the similar change in excitation. Perhaps due to the simple support bearing damping, the measured nonlinear responses at high frequencies are suppressed more than the analytical and numerical methods predict in their respective characterizations.

Yet, at low frequencies, the measurements in Fig. 7(a) directly reveal both of the snap-through dynamic regimes predicted by the analysis and simulation. The first of these is denoted with the label A, and a time series of the corresponding beam displacements operating under this steady-state is given in Fig. 8(a). Here, at 14 Hz, the beams snap-through in-phase with a progressively increasing phase delay observed in the maxima from beam 1 to 2 to 3. This phase delay is logical since small inherent damping in the system coupling springs prevents an immediate transfer of energy from the input at beam 1 through the three DOF multistable system. The second, measured snap-through regime, also predicted by the analysis and simulation, is shown in Fig. 8(b) which corresponds to the label B in the velocity amplitude plot Fig. 7(a). The time series Fig. 8 (b) reveals out-of-phase motion between beam 1, which snaps through at a frequency equal to the excitation, and beams 2 and 3 that indeed snap-through but instead at a period twice the excitation period. This explains the reduced amplitude of the far-from-equilibrium responses for beams 2 and 3 shown in Fig. 6(a) at label B$*$ and Fig. 7(a) at label B: the snap-through responses of beams 2 and 3 occur at one-half of the frequency so that the spectral component proportional to the excitation frequency, i.e. that plotted in Figs. 6(a) and 7(a), is reduced. The qualitative character of these strongly nonlinear and far-from-equilibrium dynamics is shared among analysis, simulation, and experiment, which serves as further verification and validation for the analytical model formulation.

The input and transfer impedances corresponding to the snap-through dynamic regime are presented in Figs. 6(b) and 7 (b). For ease of relating the influence of changing excitation frequency to change in the resistances and reactances, the arrows in Fig. 6(a) correspond to the arrows provided in Fig. 6(b), while in Figs. 6 and 7 the grey- and black-filled data points respectively correspond to lower and upper bound frequencies of snap-through regimes. The amplitudes of the input and transfer impedances corresponding to the snap-through regime, previously labeled by A$*$ and A, are found to be very low when compared to the intrawell responses in the quasi-linear regime results in Figs 4 and 5. This finding is intuitive since snap-through pertains to large amplitude dynamics and, as such, for a similar amount of input force the sub-system velocities are large, which corresponds to low impedance amplitudes and contrasts with the impedance amplitudes of the quasi-linear regime. As the harmonic excitation frequency driving the three DOF system increases towards the bifurcation from one snap-through regime A to the second B shown by the light cyan arrow in Fig. 7, the measurements indicate that the resistances of each sub-system reduce from small positive values towards zero while the reactance of beam 1 trends towards zero at the bifurcation. Similar trends are borne out in the analysis and simulation, respectively from the labels A$*$ to B$*$ in Fig. 6.

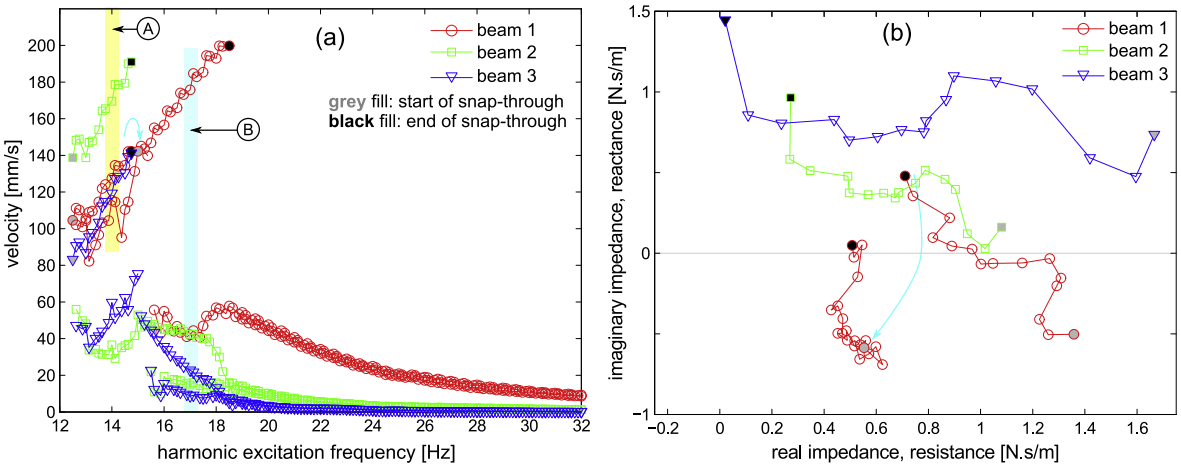

Fig. 7. Experimental results. (a) Velocity amplitude of the beams as a function of harmonic excitation frequency. (b) Trends in impedance. Only impedance measures corresponding to snap-through dynamic regimes are shown. Shaker acceleration amplitude $A = 9.3\ \mathrm{m/s^2}$. Grey- and black-filled data points respectively correspond to lower and upper bound frequencies of snap-through regimes.

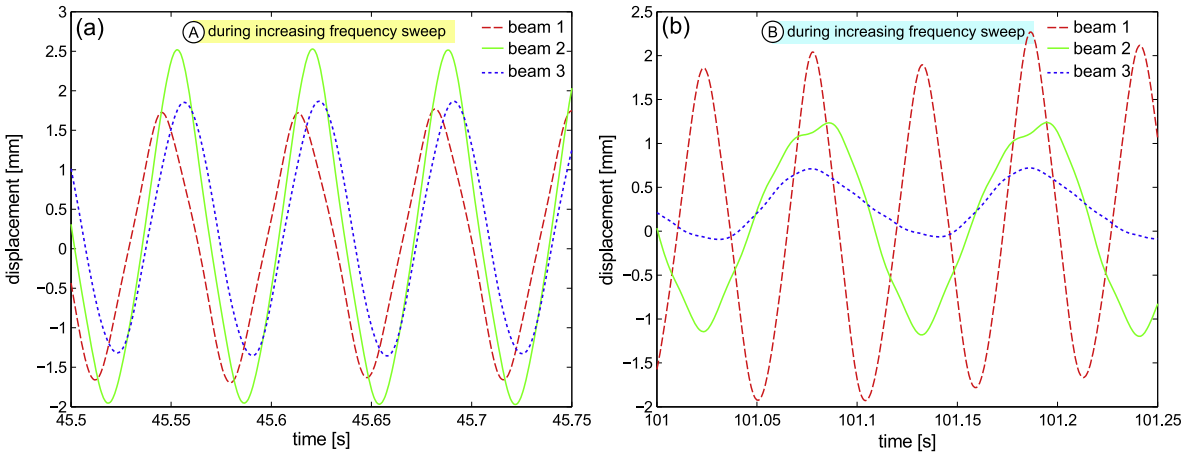

Fig. 8. Time series of beam displacements from the experimental setup. (a) and (b) show respective snap-shots of the displacements according to the labels A and B indicated in Fig. 7.

This discovery is interesting in light of the interpretation about energy management in the multi DOF system subjected to harmonic excitation force. Considering the snap-through response as a class of strongly nonlinear "resonance" since the reactance vanishes at the bifurcation point, the resistance is all that remains in the system to manage the energy that is injected into the system. Otherwise, without resistance, a system driven under a resonant state will have infinite growth in response [41]. Based on the experimental, analytical, and numerical findings, one concludes that the loss of dynamic stability for snap-through regimes of oscillation is due to the inability to balance the input driving energy with dissipation mechanisms. There is logic to this conclusion, considering prior findings that correlate increased damping to increased sustainability of snap-through response in post-buckled vibration energy harvesting platforms [44] and discoveries that increased damping promotes the formation of well-developed strange attractors [45].

A practical consequence to this conclusion is to suggest that multi DOF structures operated in conditions that potentially induce post-buckling among constituents, such as in Fig. 1(a), should be lightly damped to prevent the triggering of adverse, steady-state snap-through response. While this suggestion does indeed follow the new discoveries of this work enabled by complementary analytical, numerical, and experimental examples, it conflicts with reported evidence that lightly damped, post-buckled, built-up structures regularly undergo *transient* snap-through response, oftentimes associated with chaos [14,24]. Whether transient or steady-state, far-from-equilibrium dynamics that result in large stresses in structural systems are nevertheless to be avoided for the long-term integrity of the platform. Yet, due to the relatively straightforward means by which to measure impedance in practice, the shifts in reactance and resistance can potentially be used as real-time indicators for triggering detrimental steady-state responses as guided by the model predictions enabled by the analytical method established here.

5. Conclusions

Verified by simulations and qualitatively validated by experiments, the semi-analytical modeling approach introduced here provides efficient means to predict far-from-equilibrium, steady-state dynamics in harmonically excited, multi DOF, multistable structural systems and enables future, detailed explorations of impedance measures and energy flow in multistable structures. Characteristics in the response amplitudes and impedances for low amplitude and far-from-equilibrium dynamics regimes are faithfully predicted by the analytical approach, while intriguing details observed in the corresponding experimental platform are found to correlate well with analytical results. Future studies will uncover a refined picture of how impedance measures are tailored according to system and excitation parameters to begin formulation of guidelines for the design and deployment of built-up, multistable structural systems.

Acknowledgements

The authors are grateful for helpful conversations with Dr. S.M. Spottswood at the Air Force Research Laboratory, Structural Sciences Center, in the formulation and assessment of this research. R.L.H. acknowledges start-up funds from the Department of Mechanical and Aerospace Engineering at The Ohio State University (OSU). B.A.G. acknowledges support from the U.S. Department of Defense Science Mathematics and Research for Transformation (SMART) Scholarship and from the OSU College of Engineering Honors Research Scholarship.

References

[1] A.G. Kelkar, S.M. Joshi, Control of Nonlinear Multibody Flexible Space Structures, Springer, Berlin, 1996.
[2] R. Hutchinson, Modern materials and their incorporation into vehicle design, in: J. Happian-Smith (Ed.), An Introduction to Modern Vehicle Design, Butterworth-Heinemann, Oxford, 2002, pp. 29–56.
[3] S.M. Spottswood, T.G. Eason, R. Chona, A structural perspective on the challenges associated with analyzing a reusable hypersonic platform, in: Proceedings of the 11th International Conference on Recent Advancements on Structural Dynamics, Pisa, Italy, 2013, pp. 1–11.
[4] B. Shekastehband, K. Abedi, Dynamic propagation of snap-through buckling in tensegrity structures, Int. J. Struct. Stab. Dyn. 14 (2014) 1350049.
[5] L.N. Virgin, Vibration of Axially Loaded Structures, Cambridge University Press, Cambridge, 2007.
[6] J. Kirshenboim, D.J. Ewins, A method for recognizing structural nonlinearities in steady-state harmonic testing, J. Vib. Acoust. Stress Reliab. Des. 106 (1984) 49–52.
[7] C. Mei, J.M. Dhainaut, B. Duan, S.M. Spottswood, H.F. Wolfe, Nonlinear random response of composite panels in an elevated thermal environment, Old Dominion University Norfolk, Virginia, USA AFRL-VA-WP-TR-2000-3049, 2000.
[8] A. delli Carri, D.J. Ewins, A systematic approach to modal testing of nonlinear structures, in: R. Allemang, J. De Clerck, C. Niezrecki, A. Wicks (Eds.), Topics in Modal Analysis Volume 7: Proceedings of the 31st IMAC Conference on Structures Dynamics, Springer, New York, 2014, pp. 273–286.
[9] S.M. Spottswood, R.J. Allemang, Identification of nonlinear parameters for reduced order models, J. Sound Vibr. 295 (2006) 226–245.
[10] S.M. Spottswood, R.J. Allemang, On the investigation of some parameter identification and experimental modal filtering issues for nonlinear reduced order models, Exp. Mech. 47 (2007) 511–521.
[11] P.L. Reu, D.P. Rohe, L.D. Jacobs, Comparison of DIC and LDV for practical vibration and modal measurements, Mech. Syst. Signal Process. (2016), http://dx.doi.org/10.1016/j.ymssp.2016.02.006.
[12] D.A. Ehrhardt, M.S. Allen, S. Yang, T.J. Beberniss, Full-field linear and nonlinear measurements using continuous-scan laser doppler vibrometry and high speed three-dimensional digital image correlation, Mech. Syst. Signal Process. (2016), http://dx.doi.org/10.1016/j.ymssp.2015.12.003.
[13] R.A. Perez, B.P. Smarslok, M.P. Mignolet, Deterministic and stochastic partial linearization approach for nonlinear reduced order models of structures, in: Proceedings of the 58th AIAA SciTech Conference, Kissimmee, Florida, USA, 2015, pp. 4982–5001.
[14] R. Wiebe, S.M. Spottswood, On the dimension of complex responses in nonlinear structural vibrations, J. Sound Vibr. 373 (2016) 192–204.
[15] B.A. Miller, J.J. McNamara, S.M. Spottswood, A.J. Culler, The impact of flow induced loads on snap-through behavior of acoustically excited, thermally buckled panels, J. Sound Vibr. 330 (2011) 5736–5752.
[16] R.L. Harne, K.W. Wang, Harnessing Bistable Structural Dynamics: For Vibration Control, Energy Harvesting and Sensing, John Wiley & Sons Ltd., Chichester, 2017.
[17] L.N. Virgin, R. Wiebe, On damping in the vicinity of critical points, Philos. Trans. Royal Soc. A 371 (2013) 20120426.
[18] G. Gatti, M.J. Brennan, I. Kovacic, On the interaction of the responses at the resonance frequencies of a nonlinear two degrees-of-freedom system, Physica D 239 (2010) 591–599.
[19] R.L. Harne, C. Zhang, B. Li, K.W. Wang, An analytical approach for predicting the energy capture and conversion by impulsively-excited bistable vibration energy harvesters, J. Sound Vibr. 373 (2016) 205–222.
[20] D.R. Johnson, R.L. Harne, K.W. Wang, A disturbance cancellation perspective on vibration control using a bistable snap-through attachment, J. Vibr. Acoust. 136 (2014) 031006.
[21] R.L. Harne, Q. Dai, Characterizing the robustness and susceptibility of steady-state dynamics in post-buckled structures to stochastic perturbations, J. Sound Vibr. 395 (2017) 258–271.
[22] L.Q. Chen, W.A. Jiang, M. Panyam, M.F. Daqaq, A broadband internally resonant vibratory energy harvester, J. Vibr. Acoust. 138 (2016) 061007.
[23] R.E. Mickens, Truly Nonlinear Oscillations: Harmonic Balance, Parameter Expansions, Iteration, and Averaging Methods, World Scientific, Hackensack, New Jersey, 2010.
[24] L.N. Virgin, Introduction to Experimental Nonlinear Dynamics, Cambridge University Press, Cambridge, 2000.
[25] J. Yang, Y.P. Xiong, J.T. Xing, Power flow behaviour and dynamic performance of a nonlinear vibration absorber coupled to a nonlinear oscillator, Nonlinear Dyn. 80 (2015) 1063–1079.
[26] B. Tang, M.J. Brennan, Steady-state analysis of nonlinear systems by the receptance harmonic balance method, in: Proceedings of the 22nd International Congress on Sound and Vibration, Florence, Italy, 2015, pp. 1–7.
[27] H. Elizalde, M. Imregun, An explicit frequency response function formulation for multi-degree-of-freedom non-linear systems, Mech. Syst. Signal Process. 20 (2006) 1867–1882.
[28] G. Kerschen (Ed.), Nonlinear Dynamics, Volume 1, Proceedings of the 33rd IMAC, A Conference and Exposition on Structural Dynamics, Springer, New York, 2015.
[29] J.T. Xing, Energy Flow Theory of Nonlinear Dynamical Systems with Applications, Springer, New York, 2015.
[30] D. Restrepo, N.D. Mankame, P.D. Zavattieri, Phase transforming cellular materials, Extreme Mech. Lett. 4 (2015) 52–60.
[31] N. Hu, R. Burgueño, Buckling-induced smart applications: recent advances and trends, Smart Mater. Struct. 24 (2015) 063001.
[32] W.X. Wang, R. Yang, Y.C. Lai, V. Kovanis, C. Grebogi, Predicting catastrophes in nonlinear dynamical systems by compressive sensing, Phys. Rev. Lett. 106 (2011) 154101.
[33] R.L. Harne, K.W. Wang, A bifurcation-based coupled linear-bistable system for microscale mass sensing, J. Sound Vibr. 333 (2014) 2241–2252.
[34] P.D. Spanos, Stochastic linearization in structural dynamics, Appl. Mech. Rev. 34 (1981) 1–8.
[35] R.L. Harne, K.W. Wang, Axial suspension compliance and compression for enhancing performance of a nonlinear vibration energy harvesting beam system, J. Vibr. Acoust. 138 (2016) 011004.
[36] R.A. Ibrahim, Friction-induced vibration, chatter, squeal, and chaos: part i: mechanics of contact and friction, Appl. Mech. Rev. 47 (1994) 209–226.
[37] J. Qiu, J.H. Lang, A.H. Slocum, A curved-beam bistable mechanism, J. Microelectromech. Syst. 13 (2004) 137–146.
[38] C.W.S. To, Nonlinear Random Vibration: Analytical Techniques and Applications, CRC Press, London, 2012.
[39] M. Allen, R.L. Mayes, D.J. Rixen (Eds.), Dynamics of Coupled Structures, Volume 4, Proceedings of the 33rd IMAC, A Conference and Exposition on Structural Dynamics, Springer, New York, 2015.
[40] J.D. Hoffman, Numerical Methods for Engineers and Scientists, Marcel Dekker Inc., New York, 2001.
[41] J.P. Salter, Steady-State Vibration, Kenneth Mason, Havant, U.K., 1969.
[42] S.S. Rao, Mechanical Vibrations, 4th ed., Pearson Prentice Hall, Upper Saddle River, New Jersey, 2004.
[43] H.R. Elizalde Siller, Non-linear Modal Analysis Methods for Engineering Structures, Imperial College London, London, 2004 (Ph.D. dissertation).
[44] R.L. Harne, M. Thota, K.W. Wang, Concise and high-fidelity predictive criteria for maximizing performance and robustness of bistable energy harvesters, Appl. Phys. Lett. 102 (2013) 053903.
[45] B.F. Feeny, C.M. Yuan, Parametric identification of an experimental magneto-elastic oscillator, J. Sound Vibr. 247 (2001) 785–806.